

Statistical Trilateration With Skew-t Distributed Errors in LTE Networks

Philipp Müller, José A. del Peral-Rosado, *Member, IEEE*, Robert Piché, *Senior Member, IEEE*,
and Gonzalo Seco-Granados, *Senior Member, IEEE*

Abstract—Localization accuracy of trilateration methods in long term evolution (LTE) cellular networks, which are based on time-of-arrival, may be highly degraded due to multipath and non-line of sight conditions in urban and indoor environments. Multipath mitigation techniques usually involve a high computational burden and require wideband signals to be effective, which limit their adoption in certain low-cost and low-power mobile applications using narrow-band signals. As an alternative to these conventional techniques, this paper analyzes an expectation maximization (EM) localization algorithm that considers the skewness introduced by multipath in the LTE ranging error distribution. The EM algorithm is extensively studied with realistic emulated LTE signals of 1.4-MHz bandwidth. The EM method is compared with a standard nonlinear least squares (NLS) algorithm under ideal simulated conditions and using realistic outdoor measurements from a laboratory testbed. The EM method outperforms the NLS method when the ranging errors in the training and test stages have similar distributions.

Index Terms—Statistical trilateration, skew-t distribution, localization, LTE, expectation maximization algorithm.

I. INTRODUCTION

MOBILE phone localization has been typically supported by Global Navigation Satellite Systems (GNSS) or network-based methods with coarse accuracy, such as cell identification (CID). But the worldwide adoption of the Long Term Evolution (LTE) in fourth-generation (4G) mobile networks is starting to change this paradigm. Complementary methods based on the trilateration of LTE pilot signals are specified in the standard [1] by the Third Generation Partnership Project (3GPP), such as the observed time difference of arrival (OTDoA) and the uplink time difference of arrival (UTDoA). These trilateration methods estimate the receiver position based on measurements of distances (ranges)

Manuscript received October 9, 2015; revised March 11, 2016 and July 7, 2016; accepted July 20, 2016. Date of publication August 3, 2016; date of current version October 7, 2016. The work of P. Müller was supported in part by the Doctoral Programme of TUT's President, in part by the Finnish Doctoral Programme in Computational Sciences, and in part by the TUT-Foundation (TTY-säätiö) for his research visit to Universitat Autònoma de Barcelona, Spain. The work of J. A. del Peral-Rosado and G. Seco-Granados was supported in part by the European Space Agency through NPI under Program 4000110780/14/NL/AK and in part by the Spanish Ministry of Economy and Competitiveness under Project TEC2014-53656-R. The associate editor coordinating the review of this paper and approving it for publication was A. Giorgetti.

P. Müller and R. Piché are with the Department of Automation Science and Engineering, Tampere University of Technology, Tampere 33101, Finland (e-mail: philipp.muller@tut.fi; robert.piche@tut.fi).

J. A. del Peral-Rosado and G. Seco-Granados are with the Department of Telecommunications and Systems Engineering, Universitat Autònoma de Barcelona, Cerdanyola del Vallès 08193, Spain (e-mail: joseantonio.delperal@uab.cat; gonzalo.seco@uab.cat).

Color versions of one or more of the figures in this paper are available online at <http://ieeexplore.ieee.org>.

Digital Object Identifier 10.1109/TWC.2016.2597836

between the receiver and base stations (BSs) with known location. The use of pilot signals with up to 20 MHz of bandwidth specified in LTE [2], e.g. cell-specific reference signal (CRS), positioning reference signal (PRS) or sounding reference signal (SRS), is of special interest for accurate positioning in urban areas, where GNSS signal availability is highly reduced.

Thanks to the tight network synchronization and coordinated transmission, the main source of positioning error using ranging-based trilateration techniques in LTE is due to multipath and non-line of sight (NLoS) conditions [3]. Many techniques have been proposed to alleviate the effect of multipath [4], [5] and for NLoS identification and mitigation, such as in [6]–[9], but they typically require a known NLoS probability or a high signal bandwidth in order to resolve multipath. The NLoS problem can also be combated by using multiple antennas within joint time-of-arrival (ToA) and angle-of-arrival (AoA) methods, such as in [10]–[14], however their use implies an extra implementation cost due to the additional hardware required [6]. Still, the most typical ranging techniques are based on the correlation of the received signal with a pilot signal and the detection of the first peak above a threshold, in order to compute the time-delay estimation (TDE) or range estimation. These techniques, called threshold-based estimators [4], perform well for moderate to high signal bandwidth, such as the common LTE system bandwidths of 5 and 10 MHz [15]. However, their multipath mitigation capabilities are significantly decreased for low signal bandwidths, such as 1.4 MHz, where multipath reflections are not individually distinguishable. The bandwidth allocated for positioning services is expected to become more limited for Internet of Things (IoT) applications in LTE-M and fifth-generation (5G) cellular networks, with the proliferation of low-cost and low-power mobile devices. This context leads to the challenging goal of finding positioning techniques able to already achieve accurate localization with 4G LTE in multipath environments for the lowest system bandwidth, i.e., by using only pilot signals over 1.4 MHz.

A complementary approach to multipath countermeasures in the ranging estimation is to make use of a more elaborate statistical signal model in the localization algorithm, as in [16] and [17]. Multipath channels introduce skewness to the error distribution of ToA or range measurements, as it has been observed in [18] and [19] for ultra-wideband (UWB) networks. Taking into account this skewed or asymmetric distribution in the localization algorithm may give better performance than a standard Nonlinear Least Squares (NLS) algorithm, which is implicitly based on a Gaussian error model.

Different non-Gaussian models for ranging errors have been proposed, including, among others, the exponential (e.g. in [8] for NLoS errors), log-normal, Weibull, generalized extreme value [20], normal-Cauchy mixture [19], and normal-exponential mixture [21] distributions. In [22] we considered the skew- t distribution as a range error model and presented an Expectation Maximization (EM) algorithm for trilateration. We also showed how the parameters of a skew- t distribution can be fitted to training data using a Gibbs sampler (GS). Furthermore, in that paper simulations in idealized trilateration models showed significant positioning accuracy improvements over a standard NLS algorithm.

We chose the skew- t distribution in [22] because of the following three desirable properties. First, the skew- t distribution is a heavy-tailed distribution, which means that it copes better with large deviations in the data than the normal distribution. Second, the skew- t distribution allows us to model asymmetry in the range error data. Third, solving the trilateration problem under the assumption of skew- t distributed ranging errors is easy to implement, because the skew- t distribution can be rewritten as a hierarchical model consisting of a normal distribution with two auxiliary parameters, which enables using a standard NLS solver in the localization task.

The third property explains why we picked the skew- t distribution over mixture models. These models might be able to model the range error distribution more precisely than the skew- t distribution. However, using them for positioning is often computationally inefficient. For example, in [18] it is shown that for a Generalized Gaussian mixture error model, which has only two Gaussian components, the computation time for solving the trilateration problem is $\mathcal{O}(2^K)$, where K is the number of measurements. The computation time with normal error model is, for comparison, $\mathcal{O}(K^2)$. Furthermore, the third property shows that the skew- t distribution is a generalization of the normal distribution.

The aim of this paper is to provide a thorough study of the applicability of skew- t range error modelling approach of [22] in a realistic trilateration setting, and in particular, to evaluate it as a multipath mitigation technique to LTE positioning effective for the lowest signal bandwidth, where multipath components are unresolvable. In this paper we fit skew- t distributions to training data from 3GPP standard channel models using the Gibbs sampler presented in [22], and analyze the EM positioning accuracy in an LTE network using outdoor ranging measurements obtained from a laboratory testbed. The assessment of this statistical trilateration technique is performed under harsh conditions by using emulated data and the lowest system bandwidth of LTE, i.e., 1.4 MHz. Thus, the practical performance of the skew- t trilateration algorithm is validated in realistic conditions.

One of the objectives of modeling the range errors as skew- t distributed is to include ranging measurements under line of sight (LoS) and NLoS in a single statistical model. Because it is challenging to distinguish LoS and NLoS channel realizations from measurements in realistic conditions, our model tries to provide a statistical characterization of the distances over a medium term, where there are periods of time of LoS and periods of NLoS. This approach results in a more

robust positioning algorithm by modeling the channel effect independently of LoS or NLoS conditions.

This paper is organized as follows. In Section II we provide a review of the essential aspects of the trilateration problem, the skew- t distribution and the fitting to experimental data using a GS, as well as a description of LTE channel models and ranging methods. Although the contents of Sections II.A and II.B can be also found in [22], we consider it pertinent to include them here to put the rest of the paper in context and make it understandable. In Section III, we present briefly the EM algorithm from [22], used for solving the trilateration problem assuming skew- t distributed errors, and the dilution of precision. We then apply in Section IV the algorithms for positioning in an LTE network. After describing the testbed, we fit parameters of skew- t and normal distributions to ranging errors from two LTE standard channel models. Subsequently, we test the EM algorithm positioning performance for both channels and compare it with the performance of a standard NLS solver. Finally, we give some concluding remarks and an outlook in Section V.

Notation: \mathbf{x} and $x_{1:d}$ denote column vectors, \mathbf{H} denotes a matrix, and underscores are used to denote random variables and random vectors in contexts where the distinction from deterministic variables is useful.

II. MODEL FOR STATISTICAL TRILATERATION IN LTE

A. Statistical Trilateration

In this paper we use the following statistical formulation of the trilateration problem [23]. Let the d -dimensional random vector $\underline{x}_{1:d} = \underline{\mathbf{x}}$ represent the unknown receiver location. The K scalar measurements are modeled as

$$\underline{y}_k | (\underline{\mathbf{x}} = \mathbf{x}) = h_k(\mathbf{x}) + \underline{v}_k \quad (1)$$

for $k \in 1, \dots, K$, where the measurement function $h_k : \mathbb{R}^d \rightarrow \mathbb{R}$ models the measurement geometry, and the additive errors $\underline{v}_1, \dots, \underline{v}_K$ are mutually independent random variables. Furthermore, $\underline{\mathbf{x}}, \underline{v}_1, \dots, \underline{v}_K$ are mutually independent.

The prior probability density function (PDF) of \mathbf{x} is denoted as $p_{\underline{\mathbf{x}}}$, and the PDF of v_k as $p_{\underline{v}_k}$. The posterior distribution of \mathbf{x} given the K -dimensional measurement vector $y_{1:K} = \mathbf{y}$ has the PDF

$$p_{\underline{\mathbf{x}}|\underline{\mathbf{y}}}(\mathbf{x}|\mathbf{y}) \propto p_{\underline{\mathbf{x}}}(\mathbf{x}) \prod_{k=1}^K p_{\underline{v}_k}(y_k - h_k(\mathbf{x})), \quad (2)$$

where \propto means ‘‘proportional to’’. A value of \mathbf{x} that maximizes (2) is called a maximum *a posteriori* (MAP) estimate. If the prior distribution is ‘‘flat’’, i.e. if $p_{\underline{\mathbf{x}}}(\mathbf{x}) \propto 1$, the MAP estimate coincides with the maximum likelihood (ML) estimate.

In trilateration, the measurement function is the Euclidean distance between the receiver and a base station at a known location \mathbf{c}_k :

$$h_k(\mathbf{x}) = \|\mathbf{x} - \mathbf{c}_k\|. \quad (3)$$

The Jacobian of $\mathbf{h} = h_{1:K}$ is the $K \times d$ matrix \mathbf{H} whose k th row is the transpose of a unit vector pointing from \mathbf{c}_k to \mathbf{x} ,

that is,

$$\mathbf{H}_{n,1:n_{\mathbf{x}}} = \frac{\partial h_n(\mathbf{x})}{\partial \mathbf{x}} = \frac{(\mathbf{x} - \mathbf{c}_n)^T}{\|\mathbf{x} - \mathbf{c}_n\|}. \quad (4)$$

B. The Skew-t Distribution

This subsection presents the skew-t distribution and some of its properties that are needed later in this paper. For a more extensive discussion we refer the reader, for example, to [24, pp. 101 ff.] and [25].

A random variable \underline{z} is said to have a skew-t distribution with location ξ , scale σ^2 , skewness λ , and ν degrees-of-freedom (DOF) if its PDF has the form

$$p_{\underline{z}}(z) = \frac{2}{\sigma} t_{\nu} \left(\frac{z - \xi}{\sigma} \right) T_{\nu+1} \left(\lambda \frac{z - \xi}{\sigma} \sqrt{\frac{\nu + 1}{\nu + \frac{(z - \xi)^2}{\sigma^2}}} \right), \quad (5)$$

where t_{ν} and $T_{\nu+1}$ denote the PDF and the cumulative distribution function (CDF) of the standardized t-distribution. The skew-t distribution is denoted $\underline{z} \sim \text{ST}(\xi, \sigma^2, \lambda, \nu)$.

For $\nu > 2$ the mean and variance of $\underline{z} \sim \text{ST}(\xi, \sigma^2, \lambda, \nu)$ are

$$\mathbb{E}(\underline{z}) = \xi + \sigma g_{\nu} \delta_{\lambda}, \quad \text{var}(\underline{z}) = \sigma^2 \left(\frac{\nu}{\nu - 2} - (g_{\nu} \delta_{\lambda})^2 \right) \quad (6)$$

where $g_{\nu} = \frac{\sqrt{\nu} \Gamma(\frac{\nu-1}{2})}{\sqrt{\pi} \Gamma(\frac{\nu}{2})}$ and $\delta_{\lambda} = \frac{\lambda}{\sqrt{1+\lambda^2}} \in (-1, 1)$.

The skew-t distribution has the following hierarchical model. Let $\underline{\tau} \sim \Gamma(\nu/2, \nu/2)$ and $\underline{w} \sim \text{N}(0, 1)$, which denote the Gamma distribution with both shape and scale $\nu/2$ and the standard normal distribution. Then $\underline{t} | (\underline{\tau} = \tau) = |\sigma \underline{w} / \sqrt{\tau}|$ is a half-normal (HN) random variable with PDF

$$p_{\underline{t}}(t) = \begin{cases} \frac{2\sqrt{\tau}}{\sigma} \phi \left(t \frac{\sqrt{\tau}}{\sigma} \right) & \text{if } t > 0 \\ 0 & \text{otherwise} \end{cases} \quad (7)$$

where ϕ denotes the PDF of the standard normal distribution. Samples from the distribution $\text{ST}(\xi, \sigma^2, \lambda, \nu)$ can be drawn from the conditional distribution

$$\underline{z} | (\underline{t} = t, \underline{\tau} = \tau) \sim \text{N} \left(\xi + \frac{\lambda t}{\sqrt{1 + \lambda^2}}, \frac{1 - \delta_{\lambda}^2}{\tau} \sigma^2 \right). \quad (8)$$

In the hierarchical representation (7 – 8), the conditional random variable $\underline{t} | (\underline{z} = z, \underline{\tau} = \tau)$ has the distribution $\text{N} \left(\delta_{\lambda}(z - \xi), \frac{1 - \delta_{\lambda}^2}{\tau} \sigma^2 \right)$ and the conditional random variable $\underline{\tau} | (\underline{z} = z)$ has the PDF

$$\underline{\tau} | (\underline{z} = z) \propto \tau^{(\nu-1)/2} \exp \left(-\frac{\tau}{2} (\eta^2 + \nu) \right) \Phi(\lambda \eta \sqrt{\tau}), \quad (9)$$

where $\eta = \frac{z - \xi}{\sigma}$ and $\Phi(\cdot)$ is the CDF of the standardized normal distribution.

C. Fitting Skew-t Parameters Using a Gibbs Sampler

For fitting the parameters of a skew-t distribution to training data we apply the Gibbs sampling algorithm [26]. This algorithm computes the statistics of the posterior distributions for the parameters given n independent ranging errors $v_j | \xi, \sigma^2, \lambda, \nu \sim \text{ST}(\xi, \sigma^2, \lambda, \nu)$.

The idea of the GS is to sample from the conditional posterior distributions for each parameter separately when sampling from the (multivariate) posterior is not feasible, which is the case in our parameter estimation problem.

The algorithm works as follows. First, initial values $\xi_{(0)}, \sigma_{(0)}^2, \lambda_{(0)}, \nu_{(0)}$ are assigned to the unknown parameters. Then the parameters are ordered and samples from the conditional distribution of each parameter given the error data $v_{1:n}$ and the current estimates of the remaining parameters are drawn. This updating process is repeated $T_0 + T$ times. The posterior means of the parameters are estimated by the empirical sample means of the last T samples; the first T_0 “burn-in” samples are discarded. Other statistics, such as the covariance and quantiles, can be computed from the samples in a similar way.

For more details on how to use GS for skew-t parameter fitting we refer the reader to [22].

D. LTE Ranging and Channels

Current and next-generation mobile cellular networks are based on LTE systems, which are standardized by the 3GPP consortium. These systems are able to provide communications and positioning services within the same signal transmission. This is possible thanks to the use of multicarrier signals, which allow a flexible allocation of resources. The downlink transmission between BS and receiver or user equipment (UE) is based on orthogonal frequency division multiplexing (OFDM) modulation. The LTE downlink also specifies the OTDoA trilateration method [1]. This positioning method uses time-delay estimates or ranging measurements performed with pilot or reference signals, such as CRS or PRS. The most common ranging estimator is based on the maximum likelihood (ML) approach as [16]

$$\hat{\tau} = \underset{\tau}{\text{argmax}} \left\{ \left| \sum_{n \in \mathcal{N}} X(k, n) \cdot b^*(k, n) \cdot e^{-j \frac{2\pi n \tau}{N}} \right|^2 \right\}, \quad (10)$$

where τ is the time-delay, $X(k, n)$ is the frequency received signal at the k -th symbol and n -th subcarrier, $b^*(k, n)$ is the conjugate of the pilot code, \mathcal{N} is the set of reference subcarriers, and N is the total number of subcarriers. However, this estimator, so-called matched filter, has a poor performance in multipath environments. Thus, threshold-based ranging estimators are typically used to mitigate multipath [4], [5]. This approach consists of finding the first resolvable path or first peak of the correlation function above a certain threshold, such as adaptive threshold or signal-to-noise ratio (SNR)-based threshold [15]. This conventional ranging estimator is used as a reference method in this paper, by considering a heuristic threshold of -6 dB with respect to the maximum of the correlation function.

LTE specifies OTDoA in [1] as a network-based trilateration method, where the receiver position is calculated at a location server. First, there is a request to locate the receiver either initiated by the network or the receiver itself. Second, the network allocates the necessary positioning resources, and the receiver obtains the ranging measurements using assistance

TABLE I
MAIN PARAMETERS OF THE STANDARD LTE CHANNEL MODELS

Tap no.	EPA channel		ETU channel	
	τ (ns)	SMR (dB)	τ (ns)	SMR (dB)
1	0	0.0	0	-1.0
2	30	-1.0	50	-1.0
3	70	-2.0	120	-1.0
4	90	-3.0	200	0.0
5	110	-8.0	230	0.0
6	190	-17.2	500	0.0
7	410	-20.8	1600	-3.0
8			2300	-5.0
9			5000	-7.0

data provided by the network. Then, the location server requests the synchronization offsets and locations of each BS. Since this information is not provided to the receiver, its position can only be computed at the location server. Finally, the estimated position is sent back to the receiver.

The 3GPP consortium defines the minimum performance requirements of the LTE standard. For this purpose, several propagation channel models have been specified for simulation and testing of the communication and positioning capabilities of this cellular system. The main channel models adopted in LTE are the Extended Pedestrian A (EPA), Extended Vehicular A (EVA) and Extended Typical Urban (ETU), which are intended to model multipath environments with low, medium and large delay spread, respectively [27]. These are tapped-delay line (TDL) models with time-varying channel coefficients with a Rayleigh fading distribution. Doppler shifts of 5 and 70 Hz are also used to represent low and high mobility conditions, resulting in the EPA5 and EVA70 or ETU70 models, respectively, whose main parameters are shown in Table I, as specified in [27, Appendix B]. These channel models do not consider distance-dependent LoS conditions, but their fading events result in a probability of NLoS around 13%, 19% and 37% for EPA5, EVA70 and ETU70, respectively, which has been calculated with 470 680 channel realizations during 336.2 seconds and a LoS threshold of -6 dB. Thus, periods of LoS and NLoS conditions are found using these channel models. Advanced channel models are also specified in the LTE standard, such as three-dimensional (3D) channel models in [28] for indoor environments, but they are out of the scope of this paper, where only outdoor macro-cell deployments are considered.

The impact of multipath on the ranging error can be approximately characterized by means of the mean delay spread, also called *center of gravity* of the channel impulse response (CIR), as in [29]. The mean delay spread is defined by the power delay profile (PDP) for each channel realisation. Fig. 1 shows the PDF of the mean delay spread for the 3GPP standard channel models, considering the power delay profiles defined in [27]. This PDF describes those tap delays with a major contribution for a given channel model. Thus, Fig. 1 can be used to define non-resolvable or close-in multipath scenarios, if most of the channel contribution is within a

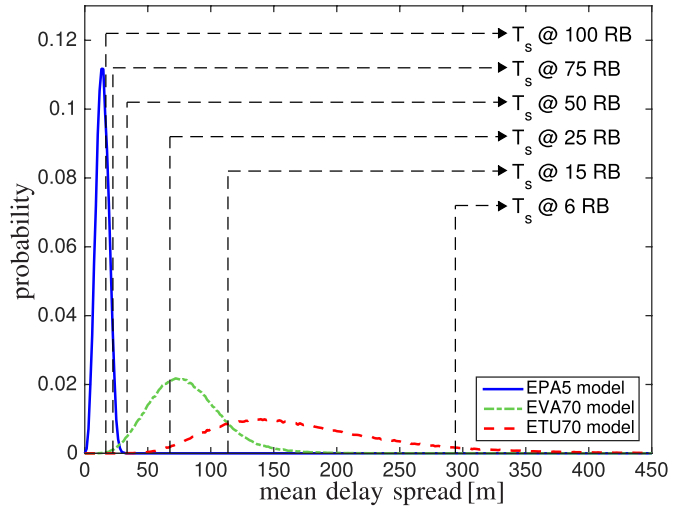


Fig. 1. PDF of the mean delay spread for EPA5, EVA70 and ETU70 channel models, computed with 470 680 channel realizations during 336.2 seconds.

sampling period T_s with respect to the LoS ray, such as EPA, EVA or ETU models for the lowest system bandwidth of LTE, i.e. 1.4 MHz with 6 resource blocks (RB). At this low bandwidth, the multipath rays are non-resolvable, and they limit the efficiency of multipath mitigation techniques. Thus, positioning algorithms, such as statistical trilateration, that are able to mitigate these effects are of special interest. These advanced algorithms are evaluated in this paper only for EPA and ETU channel, which represent mild and harsh multipath conditions, respectively, for 1.4-MHz system bandwidth, where close-in multipath is predominant.

III. ESTIMATION OF THE RECEIVER POSITION

A. Positioning Using Expectation Maximization

In this subsection, we present the basics of the EM algorithm for computing the MAP estimate $\hat{\mathbf{x}}$, i.e. the mode of (2), for additive skew-t measurement errors. The algorithm's maximization step (M-step) is the standard NLS problem. For details we refer the reader to [22].

Algorithm 1 shows the pseudo code of the method, which starts with the M-step. Given K independent scalar measurements \mathbf{y} and assuming a multivariate-normal prior distribution for \mathbf{x} with mean \mathbf{m} and covariance \mathbf{P} , the M-step is the computation of the mode of the conditional posterior $p(\mathbf{x}^{(j)} | \mathbf{y}, t_{1:K}^{(j-1)}, \tau_{1:K}^{(j-1)})$, that is,

$$\hat{\mathbf{x}} \leftarrow \underset{\mathbf{x}}{\operatorname{argmin}} \left((\mathbf{x} - \mathbf{m})' \mathbf{P}^{-1} (\mathbf{x} - \mathbf{m}) + \frac{\sum_{k=1}^K \tau_k^{(j-1)} \left(y_k - h_k(\mathbf{x}) - \zeta - \delta_\lambda t_k^{(j-1)} \right)^2}{\sigma^2 (1 - \delta_\lambda^2)} \right). \quad (11)$$

The minimization in (11) can be computed by any standard NLS algorithm; we use the descending Gauss-Newton (dGN)

Algorithm 1 Computing Position Estimate by EM

Input: $\mathbf{c}_{1:K}$, \mathbf{y} , \mathbf{m} , \mathbf{P} , n_{EM} (number of EM iterations) and n_{dGN} (number of descending-GN iterations)
Initialize $\mathbf{x}^{(0)} \leftarrow \mathbf{m}$, $t_{1:K}^{(0)} \leftarrow -\xi/\delta_\lambda$ and $\tau_{1:K}^{(0)} \leftarrow 1$
for $j = 1$ to n_{EM} **do**
 Initialize $\hat{\mathbf{x}} \leftarrow \mathbf{x}^{(j-1)}$, compute $\tilde{\mathbf{y}} \leftarrow \mathbf{y} - \xi - \delta_\lambda t_{1:K}^{(j-1)}$
 and $\mathbf{R} \leftarrow \sigma^2(1 - \delta_\lambda^2)\text{diag}\{1/\tau_1^{(j-1)}, \dots, 1/\tau_K^{(j-1)}\}$
 for $i = 1$ to n_{dGN} **do**
 Compute $\mathbf{H} \leftarrow \frac{\partial \mathbf{h}_{1:K}}{\partial \mathbf{x}}(\hat{\mathbf{x}})$ using (4)
 Compute $\mathbf{K} \leftarrow \mathbf{P}\mathbf{H}^T(\mathbf{R} + \mathbf{H}\mathbf{P}\mathbf{H}^T)^{-1}$ and
 $\mathbf{d}_{GN} \leftarrow \mathbf{m} - \hat{\mathbf{x}} + \mathbf{K}(\tilde{\mathbf{y}} - \mathbf{h}(\hat{\mathbf{x}}) - \mathbf{H}\mathbf{m} + \mathbf{H}\hat{\mathbf{x}})$ (or
 $\mathbf{d}_{GN} \leftarrow (\mathbf{H}^T\mathbf{R}^{-1}\mathbf{H})^{-1}\mathbf{H}^T\mathbf{R}^{-1}(\mathbf{h}(\hat{\mathbf{x}}) - \tilde{\mathbf{y}})$ if
 $\mathbf{P}^{-1} = \mathbf{0}$, i.e. if prior is flat)
 Compute $f(\hat{\mathbf{x}})$ using (12) with $\mathbf{x} \leftarrow \hat{\mathbf{x}}$
 Set $\alpha \leftarrow 1$ and compute $f(\hat{\mathbf{x}} + \alpha\mathbf{d}_{GN})$ using (12)
 with $\mathbf{x} \leftarrow \hat{\mathbf{x}} + \alpha\mathbf{d}_{GN}$
 while $f(\hat{\mathbf{x}} + \alpha\mathbf{d}_{GN}) \geq f(\hat{\mathbf{x}})$ **do**
 Set $\alpha \leftarrow \alpha/2$, and compute $f(\hat{\mathbf{x}} + \alpha\mathbf{d}_{GN})$ using
 (12) with $\mathbf{x} \leftarrow \hat{\mathbf{x}} + \alpha\mathbf{d}_{GN}$
 end while
 Set $\hat{\mathbf{x}} \leftarrow \hat{\mathbf{x}} + \alpha\mathbf{d}_{GN}$
 end for
 Set $\mathbf{x}^{(j)} \leftarrow \hat{\mathbf{x}}$ and compute for $k = 1, \dots, K$

$$\tau_k^{(j)} \leftarrow \frac{\sigma^2(1 - \delta_\lambda^2)v^2}{(y_k - h_k(\mathbf{x}^{(j)}) - \xi - \delta_\lambda t_k^{(j-1)})^2 + 4\sigma^2(1 - \delta_\lambda^2)}$$

$$t_k^{(j)} \leftarrow \mu_k + \sigma_k \sqrt{\frac{2}{\pi}} / \text{erfcx}\left(\frac{-\mu_k/\sigma_k}{\sqrt{2}}\right)$$
 where scaled complementary error function
 $\text{erfcx} \leftarrow \exp(x^2)\text{erfc}(x)$ and

$$\mu_k \leftarrow \frac{1}{2\delta_\lambda} (y_k - h_k(\mathbf{x}^{(j)}) - \xi), \sigma_k \leftarrow \sqrt{\frac{\sigma^2(1 - \delta_\lambda^2)}{2\tau_k^{(j)}}}$$
end for

algorithm (see e.g. [23]). The dGN gets its name from the scaling factor α seen in Algorithm 1, which ensures a decreasing cost function

$$f(\mathbf{x}) = \frac{1}{2} \left((\mathbf{x} - \mathbf{m})' \mathbf{P}^{-1} (\mathbf{x} - \mathbf{m}) + (\mathbf{h}(\mathbf{x}) - \tilde{\mathbf{y}})^T \mathbf{R}^{-1} (\mathbf{h}(\mathbf{x}) - \tilde{\mathbf{y}}) \right), \quad (12)$$

where $\tilde{\mathbf{y}} = \mathbf{y} - \xi - \delta_\lambda t_{1:K}^{(j-1)}$ and $\mathbf{R} = \sigma^2(1 - \delta_\lambda^2)\text{diag}\{1/\tau_1^{(j-1)}, \dots, 1/\tau_K^{(j-1)}\}$. The scaling factor α is found by line search.

Using (8), a hierarchical version of the measurement model $y_k | (\mathbf{x} = \mathbf{x}) \sim \text{ST}(\xi + h_k(\mathbf{x}), \sigma^2, \lambda, v)$ is

$$y_k | (\mathbf{x} = \mathbf{x}, t_k = t_k, \tau_k = \tau_k) \sim \text{N}\left(\xi + h_k(\mathbf{x}) + \delta_\lambda t_k, \frac{1 - \delta_\lambda^2}{\tau_k} \sigma^2\right), \quad (13)$$

where the hyperparameters are $t_k | (\tau_k = \tau_k) = |\sigma \underline{w}_k / \sqrt{\tau_k}|$ with $\underline{w}_k \sim \text{N}(0, 1)$ and $\tau_k \sim \Gamma(v/2, v/2)$. In the EM algorithm's expectation step (E-step) the hyperparameters are updated by setting them to the mean values of their conditional distributions. For $t_k^{(j)}$ the conditional distribution is a truncated normal distribution that rejects negative values, with center

$\mu_k = \frac{1}{2\delta_\lambda} (y_k - h_k(\mathbf{x}) - \xi)$ and scale $\sigma_k = \sqrt{\frac{\sigma^2(1 - \delta_\lambda^2)}{2\tau_k^{(j)}}}$; for $\tau_k^{(j)}$ the conditional distribution is a Gamma distribution with shape parameter $v/2$ and scale parameter

$$\frac{2\sigma^2(1 - \delta_\lambda^2)v}{(y_k - h_k(\mathbf{x}^{(j)}) - \xi - \delta_\lambda t_k^{(j-1)})^2 + 4\sigma^2(1 - \delta_\lambda^2)}.$$

In Algorithm 1, the update formula for t_k is written using the scaled complementary error function erfcx , a special function defined as $\exp(x^2)\text{erfc}(x)$ that is available in mathematical software libraries. The update formula presented in [22] is mathematically equivalent but gives significant numerical floating point computation errors for large negative values of μ_k/σ_k .

Since the trilateration problem in real-world applications usually has to be solved in real time in mobile devices, the EM algorithm rate of convergence is important. The EM algorithm is known to converge very slowly for some problems. However, according to Xu and Jordan [30], for such problems also other gradient-based methods generally show slow convergence. They also state that the EM converges monotonically without requiring the user to set a learning rate, a property that not all alternative approaches have. Dempster *et al.* [31] show that the algorithm converges with a linear rate and that this rate depends on the amount of information inherent in the measurements. Our tests for [22] showed that for the trilateration problem the EM algorithm converges quickly; four iterations were enough to converge to the EM's position estimate.

If one is interested in the posterior mean and its covariance rather than the posterior mode for the position estimate then a Gibbs sampler [26] instead of the EM algorithm can be applied. However, the GS is significantly slower than the EM algorithm, because it requires significantly more samples (called iterations in the EM). In order to achieve the same positioning accuracy as the EM method within the test framework of [22] we had to use $T_0 = 500$ burn-in and $T = 1000$ retained samples, which resulted in a 400 times higher computation time for the GS compared with the EM. While for fitting parameters of skew-t distributions, which usually is done offline, the running time is of secondary importance and confidence intervals for the estimated parameters are more relevant, for online positioning this increase in computation time prohibits real-time positioning.

B. Dilution of Precision

The precision of a trilateration algorithm is highly affected by the location of the receiver and BSs, which is defined by the geometry matrix $\mathbf{H}_{k,1:d}$ in (4). The position dilution of precision (PDOP) is a metric to assess the geometry quality of a certain position determination, which is written in [32, p.149] as

$$\text{PDOP} = \sqrt{\text{trace} \left\{ \left(\mathbf{H}_{k,1:d}^T \mathbf{H}_{k,1:d} \right)^{-1} \right\}}. \quad (14)$$

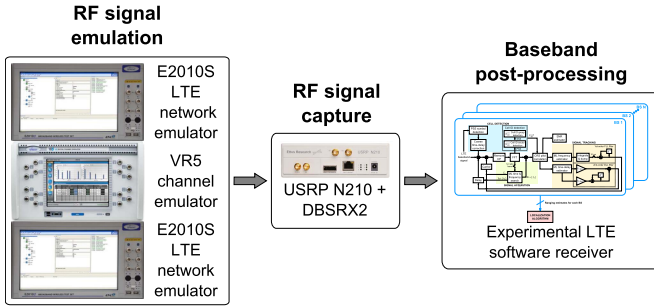


Fig. 2. LTE positioning testbed at ESA's Navigation Laboratory.

The PDOP measures the confidence level of the position determination. A good geometry can be considered for PDOP values below 5, being excellent below 2.

IV. RESULTS

This section assesses the performance of the EM and dGN algorithms in realistic LTE conditions. For this purpose, experimental results of these statistical trilateration techniques are obtained by emulating real LTE signals and using an LTE software receiver. The position accuracy is assessed by considering the impact of multipath, propagation losses, and geometry between mobile device and BS. Further ranging impairments, such as shadowing, interference, or network synchronization errors, have not been considered, in order to focus on the assessment of the multipath counteraction capabilities of the proposed positioning algorithm. The standard channel models EPA and ETU are used to characterize the multipath environments for the sake of reproducibility.

A. Explanation of the Testbed

The experimental results obtained in this paper are based on the ranging measurements computed in an LTE testbed of the European Navigation Laboratory (ENL) at the European Space Agency (ESTEC, The Netherlands). As is shown in Fig. 2, this testbed is divided into three parts:

- 1) *RF signal emulation*: LTE downlink signals are emulated at a certain RF band by means of the two Spirent E2010S network emulators, which are able to generate signals for up to 4 BSs. The channel effects are generated with a Spirent VR5 HD spatial channel emulator. The power of the received signals relative to the location of the receiver and BSs are applied according to pre-computed values with an LTE network simulator, such as in [33] and in [34]. The distance-dependent propagation losses are modeled according to the standard macro-cell layout in [35], without considering the effect of shadowing. The standard multipath channel models are then added to each downlink signal.
- 2) *RF signal capture*: the RF emulated signal is down-converted to baseband with a software-defined radio (SDR), i.e., USRP N210 with DBSRX2 daughterboard, which is a reconfigurable RF front-end. Then, the LTE baseband signal is digitized and transferred to a computer, which stores the real and imaginary part of the

captured samples in a file. An active hydrogen maser is used as an external reference clock for the SDR by generating a very stable 10-MHz reference signal.

- 3) *Baseband post-processing*: the baseband samples are post-processed with an experimental LTE software receiver in MATLAB. As is described in [36], the main modules of this LTE software receiver are the cell detection, acquisition, tracking, and positioning.

The testbed is configured to transmit up to 4 BSs on the LTE band 20, corresponding to a carrier frequency of 816 MHz, with a bandwidth of 1.4 MHz. The emulated network of BSs is tightly synchronized by the equipment, achieving a delay within one sample between the radio frames transmitted by different BSs. Since the aim of the paper is to assess the multipath counteraction capabilities of the proposed positioning algorithm, the test experiment is designed to avoid and remove additional impairments, such as interference, synchronization offsets or tracking errors, which can induce loss of lock. Thus, one BS is used to generate LTE signals with a high SNR over an additive white Gaussian noise (AWGN) channel (that is, with LoS conditions). Then, the signal tracking of this BS allows a complete calibration and control of the testbed. The rest of the BSs can be configured to emulate a specific scenario, by varying the multipath environment and the received power level. The delay corresponding to the signal time-of-flight between BS and receiver is not emulated in order to avoid synchronization and inter-cell interference errors at the receiver. The EPA5 and ETU70 models are here used to cover as many realistic scenarios as possible. The EPA5 model is aimed to represent open environments and pedestrians walking, whereas the ETU70 model is aimed to represent urban environments with high mobility. The NLoS probability due to multipath fading is approximately 13% and 37% for EPA5 and ETU70 channel models, respectively.

The tests are conducted in two sequential phases: calibration and testing of the receiver. During the calibration phase, LoS conditions are emulated for every channel. This allows the receiver to estimate the network clock offsets. These clock offsets, which are typically within 10ns, are obtained by averaging the time-delay estimates over the calibration period, i.e., 5 seconds in Section IV-B and 30 seconds in Section IV-D, approximately. During the testing phase, one BS remains in the same LoS conditions, while the specific multipath contribution is reestablished on the rest of emulated channels. This phase is used to test the trilateration algorithms proposed.

The LTE signals are captured by the USRP at a sampling frequency of 2 MHz with a gain of 31 dB. Then, the LTE baseband software receiver loads the data file of the signal capture and downsamples the signal to 1.92 MHz. The cell detection and acquisition is aided with the known cell ID of each BS. Given the tight network synchronization, signal tracking is entirely driven by the BS that only transmits high-SNR signals over an AWGN channel. The accurate time-delay and frequency estimates obtained using this BS provides tracking updates to the remaining BSs, which are transmitting LTE signals over multipath channels. Thus, one of the BSs is dedicated for accurate signal tracking, while the rest of BSs are used to obtain ranging measurements.

The tracking architecture of the LTE software receiver is based on a delay lock loop (DLL) and a frequency lock loop (FLL), as it is described in [37]. These tracking loops use the ML time-delay estimator and a usual frequency estimator [37]. The ranging measurements are obtained with a threshold-based estimator, as a conventional technique to mitigate multipath [4], [15]. The first path detection is defined by a threshold of 6 dB below the maximum correlation peak. The TDE range is bounded to one sampling period T_s (i.e., $[-0.5T_s, 0.5T_s]$) for both EPA5 and ETU70 models, as in [16]. In addition, the multipath impact of ETU70 model is assessed for an extended boundary of $[-0.5T_s, 6T_s]$. Only 14 out of 40 CRS symbols per radio frame are considered, which are those aligned in the same subcarrier positions and with low inter-cell interference. These pilot symbols are used for TDE and frequency estimation, as well as for SNR estimation with the non-data-aided technique presented in [38]. Considering only the BS dedicated for signal tracking, its time-delay and frequency offset estimates are averaged every radio frame and filtered within the tracking loops. The sampling period of the loops T_L is then equal to 10 ms, and the noise bandwidth B_L is set to 10 Hz and 5 Hz for the DLL and FLL, respectively.

The ranging measurements are compensated by the network clock offsets computed during the calibration phase. These clock offsets include the time delay between the transmission time of the BSs, with respect to the local oscillator of the SDR. Thus, the compensated time-delay estimates are directly assigned to the ToA measurements, without any impact from synchronization or tracking errors. In order to emulate the receiver location, the corresponding distance between receiver and BS is added to the ToA measurements. Thus, the performance of the statistical trilateration techniques is only affected by multipath, noise, and the geometry of the network.

B. Fitted Distributions for Standard 3GPP Channel Models

In this section, we fit the parameters of a skew-t distribution to training data consisting of ranging errors from the two 3GPP channel models EPA5 and ETU70, with TDE ranges limited to the intervals $[-0.5, 0.5]$ and $[-0.5, 6]$ in T_s units, and nominal SNR around 24 dB. For comparison, we fit a normal distribution to the training data as well and compute for both fitted distributions the Kullback-Leibler divergence (KLD, see e.g. [39]) and the Jensen-Shannon divergence (JSD, see e.g. [40], [41]).

The training data consists of $n = 56000$ ranging errors for each of the two channel models, which are computed in separate tests. Two BSs are emulated for each test. The signal from the first BS is the most powerful and it is affected only by the AWGN channel. This signal is used for calibration and tracking purposes in the coupled architecture described in the previous section. The second BS is received with a lower power level, and it is affected by EPA5 or ETU70 channel. For estimating the parameters of the skew-t distribution, the hierarchical model (7 – 8) and JAGS [42], which is a program that allows analyzing Bayesian hierarchical models by Gibbs samplers, are used with the second BS signal. We run the GS,

TABLE II
PARAMETER STATISTICS OF NORMAL AND SKEW-t DISTRIBUTIONS
FITTED TO RANGING ERROR DATA FROM EPA5 AND ETU70
CHANNEL MODELS.

Channel & TDE	Distr.	Para.	5%-ile	Mean	95%-ile
EPA5 [-0.5, 0.5]	normal	μ	15.4732	15.6604	15.8476
		σ_N	22.4680	22.5996	22.7327
	skew-t	ξ	15.8720	16.0729	16.2699
		σ	9.1785	9.2501	9.3272
		λ	-0.0487	-0.0258	-0.0035
		ν	2.0002	2.0031	2.0092
ETU70 [-0.5, 0.5]	normal	μ	54.9449	55.4001	55.8553
		σ_N	54.6397	54.9596	55.2834
	skew-t	ξ	91.0094	96.4622	99.2513
		σ	53.1084	58.2403	60.8023
		λ	-1.3885	-1.2580	-1.0117
		ν	5.8413	7.3108	8.1241
ETU70 [-0.5, 6]	normal	μ	67.9532	68.5548	69.1563
		σ_N	86.1217	86.5449	86.9725
	skew-t	ξ	51.6111	52.3925	53.1493
		σ	37.2048	37.5355	37.8999
		λ	0.2322	0.2528	0.2747
		ν	2.0550	2.0876	2.1222

as explained in Section II.C, twice with the initial parameter estimates $\zeta_{(0)}$ set to the empirical mean and $\sigma_{(0)}^2$ set to the empirical variance of the errors; $\lambda_{(0)}$ is set to 0 and 1, and $\nu_{(0)} = 5$ for both runs. In both runs we use 200 “burn-in” and 500 retained samples. For each parameter, we apply a diffuse prior; only for ν a slightly informative prior, namely a uniform distribution over the interval (2, 100) is used because $\nu > 2$ is necessary for the existence of variance.

The parameters of the normal distribution (mean μ and standard deviation σ_N) are fitted by maximum likelihood, which does not require any initial parameter estimates.

Table II contains the estimate statistics for the parameters of both fitted distributions. Column *Mean* shows the mean estimate, and columns *5%-ile* and *95%-ile* show the 5 and 95 percentiles of each parameter.

Due to the large amount of training data the parameter estimates yielded by the applied methods are very certain for all parameters; the differences between the values in *Mean*, *5%-ile* and *95%-ile* are small.

For the EPA5 channel model, the ranging errors are unskewed, which causes similar values for the estimates of the normal distribution’s mean μ and the skew-t distribution’s location ξ . However, the PDF of the two fitted distributions differ significantly (see upper plot in Fig. 3). While the normal distribution (black dashed line) is unable to capture the normalized error histogram’s heavy tails and the concentration of probability mass around its peak, the skew-t distribution (blue line) captures the shape almost perfectly. This behavior could be expected due to the small value of the estimated DOF ν . Both KLD and JSD are smaller for the fitted skew-t distribution, meaning that it is a better fit than the normal distribution.

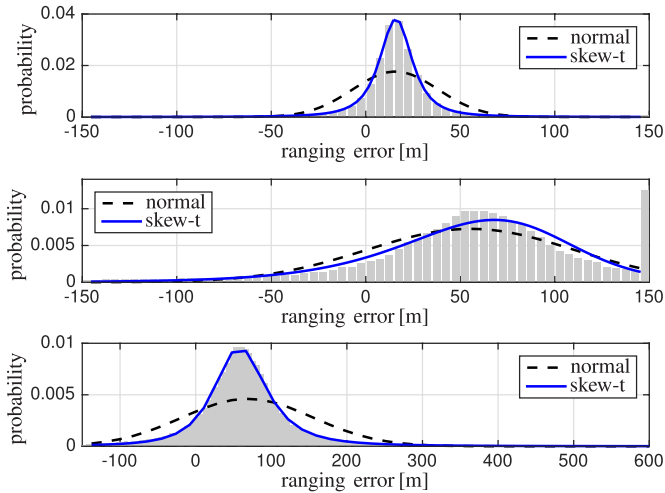


Fig. 3. Ranging error histograms with fitted normal and skew-t distributions for EPA5 channel model (upper), ETU70 channel model with TDE $[-0.5T_s, 0.5T_s]$ (middle), and ETU70 channel model with TDE $[-0.5T_s, 6T_s]$ (lower, errors above 600 meters are not displayed).

The normalized histograms of ranging errors from the ETU70 channel model for both TDE ranges also lack significant skewness (see middle and lower plots in Fig. 3). For TDE range $[-0.5T_s, 0.5T_s]$ the errors are more evenly spread than for EPA5. Thus, it is not surprising that the PDFs of both fitted distributions captures the histogram’s shape well. Although the (unskewed) t-distribution approaches the normal distribution only as ν approaches infinity, already for values around 20, there is hardly any visible difference between a t-distribution and a normal distribution with same mean and scale. This and the small skewness, explains that both normal and skew-t fits are looking similar for the ETU70 channel. For both distributions the KLD and JSD values differ less strongly than for the EPA5 data, although skew-t is still the better fit but by a smaller margin.

The huge amount of errors in the right-most bin was expected, because the estimator works within a small range (within one sampling period). Therefore, any error out of the estimation boundaries will appear at the boundary value. The cause for error beyond the estimation boundaries is multipath.

For the ETU70 channel model with TDE range $[-0.5T_s, 6T_s]$ the skew-t distribution (blue line) is a better fit than the normal distribution (black dashed line); its KLD and the JSD values are smaller than the values of the normal distribution. The lower plot in Fig. 3 shows only ranging errors up to 600 meters, although the calibration data contains errors of up to 1523 meters. However, these errors are few and hardly visible in the histogram.

C. Numerical Experiment

Here we test the positioning with the EM algorithm for the EPA5 and ETU70 channel models with TDE ranges $[-0.5T_s, 0.5T_s]$ and $[-0.5T_s, 6T_s]$, under the premise that ranging errors are skew-t distributed with the parameters given in column *Mean* of Table II. We compare the EM algorithm with the standalone dGN, which assumes normal distributed

TABLE III
POSITIONING ERROR QUANTILES FOR NUMERICAL EXPERIMENT WITH ADDITIVE SKEW-t MEASUREMENT ERRORS WITH THE DISTRIBUTION’S PARAMETERS TAKEN FROM COLUMN *Mean* OF TABLE II

Channel	TDE range	Method	50%-ile	67%-ile	95%-ile
EPA5	[-0.5,0.5]	NLS	9.18	11.17	20.14
		EM	6.24	8.01	17.89
ETU70	[-0.5,0.5]	NLS	39.35	46.43	76.91
		EM	22.44	30.64	68.04
ETU70	[-0.5,6]	NLS	23.96	32.46	77.89
		EM	23.95	30.76	72.93

errors. To avoid confusion, we use in the following NLS for the standalone dGN, and dGN for referring to the descending Gauss-Newton used inside the EM.

The aim of the numerical experiment is to discover how both algorithms perform under perfect conditions in which measurement errors in calibration data and testing data are identically distributed. We will use the results in the next subsection to analyze both algorithms’ performances when applied to emulated data, where the assumption of identical error distribution in general does not hold.

For this test, we use a similar setup as in [22]. In this section \mathbf{x} is a two-dimensional position and we assume it has the prior distribution

$$\mathbf{x} \sim \text{MVN}(\mathbf{m}, \mathbf{P}) = \text{MVN}\left(\begin{bmatrix} 0 \\ 0 \end{bmatrix}, 1000\mathbf{I}_{2 \times 2}\right), \quad (15)$$

where $\text{MVN}(\cdot, \cdot)$ denotes a bivariate Gaussian distribution with given mean and covariance matrix. Four BSs are located at the corners of a 1000-by-1000 square centered at \mathbf{m} , resulting in an excellent geometry with PDOP values below 2 inside the square.

For each channel model and TDE range, 1000 receiver positions are drawn from the prior distribution (15). Using (3) for computing the true distance $h_k(\mathbf{x})$ between the receiver position and the BS location, $K = 12$ independent distance measurements (three to each BS) are drawn from $y_k | (\mathbf{x} = \mathbf{x}) \sim \text{ST}(\xi + h_k(\mathbf{x}), \sigma^2, \lambda, \nu)$.

The hyperparameters used in the EM by the hierarchical version (13) of the measurement model are initialized as $\tau_k \leftarrow 1$ and $t_k \leftarrow -\xi_{\text{Median}} / \delta_{\lambda_{\text{Median}}}$, which ensures that the dGN finds the minimizer of the likelihood for Gaussian noise. For the EM algorithm 4 iterations are performed, and in each M-step 4 iterations of the dGN algorithm are performed. The NLS used for comparison also runs 4 iterations. In both the EM and the NLS algorithms the number of repetitions to find a suitable scaling factor α is limited to 5.

Table III presents the error statistics for both algorithms. The *50%-ile*, *67%-ile* and *95%-ile* are the quantiles of all positioning errors, which are defined as the Euclidean distance (cf. (3)) between the true position \mathbf{x} and the position estimate $\hat{\mathbf{x}}$. The EM algorithm has always approximately five times higher computation time than the NLS, as explained in [22].

For all three cases EM outperforms NLS in each of the three error statistics. But rates of improvement differ significantly. While the error quantiles for the EPA5 channel and ETU70

channel with TDE range $[-0.5 T_s, 0.5 T_s]$ are significantly reduced, the improvements for the ETU70 channel with TDE range $[-0.5 T_s, 6 T_s]$ are less significant.

It is important to note that we neglect the influence of the SNR in this test. That is, SNR is arbitrarily high and there is only a multipath and geometrical impact on the receiver localization, hence without considering the variation of received power with distance between the receiver and the BS. In the following section, a more realistic scenario is considered, where the SNR varies depending on the receiver distance.

D. Test With Real-World Emulated Data

Real-world conditions are tested in this section by emulating an LTE macro-cell deployment using the testbed described in Section IV-A. Most of the possible receiver locations are tested by considering the received power at each point and EPA5 or ETU70 channel models. The performance and computational complexity of the EM and NLS algorithms are then assessed.

The test is based on an LTE network deployment over a 2km-by-2km area with seven BSs. This is the typical cell layout specified in [35] with three-sectorial macro-cells (i.e. 3 dB-beamwidth corresponding to 65 degrees), located in a hexagonal grid with inter-site distance of 750 meters (the arrangement of BSs can be seen in Fig. 10). The PDOP values of this deployment are between 1 and 2, resulting in an excellent geometry for positioning. The receiver locations are defined in a grid of 50m squares, resulting in 1 681 grid points. The received signal power from each BS is computed as in [34], considering the standard network parameters in [35]. Since only ranging measurements from the three most powerful BSs are considered for each grid point, without loss of realism, only three BSs are emulated over EPA5 or ETU70 multipath channels for positioning purposes, while using one extra BS over AWGN channel for tracking purposes.

The LTE software receiver provides 280 measurements at each grid point, because there are 14 measurements per radio frame and 20 radio frames per grid point. Determining one position estimate uses four ranging measurements per BS, meaning that a total of 12 measurements are used in the EM or NLS algorithm. Given the 280 measurements per BS, we are able to compute 70 position estimates per grid point. The average of these estimates is then used to obtain the positioning error in that grid point.

For the EM algorithm, we assume ranging measurements being distributed as

$$y_k|\mathbf{x} \sim \text{ST}\left(\xi_{\text{Mean}} + h_k(\mathbf{x}), \sigma_{\text{Mean}}^2, \lambda_{\text{Mean}}, \nu_{\text{Mean}}\right), \quad (16)$$

and for the NLS algorithm, we assume ranging measurements being distributed as

$$y_k|\mathbf{x} \sim \text{N}\left(\mu_{\text{Mean}} + h_k(\mathbf{x}), \sigma_{N_{\text{Mean}}}^2\right), \quad (17)$$

where the parameter values are taken from column *Mean* in Table II.

We modify both methods such that the number of iterations in EM n_{EM} , in its dGN n_{dGN} , and in NLS n_{NLS} are not fixed but rather using threshold values. If the position estimates of

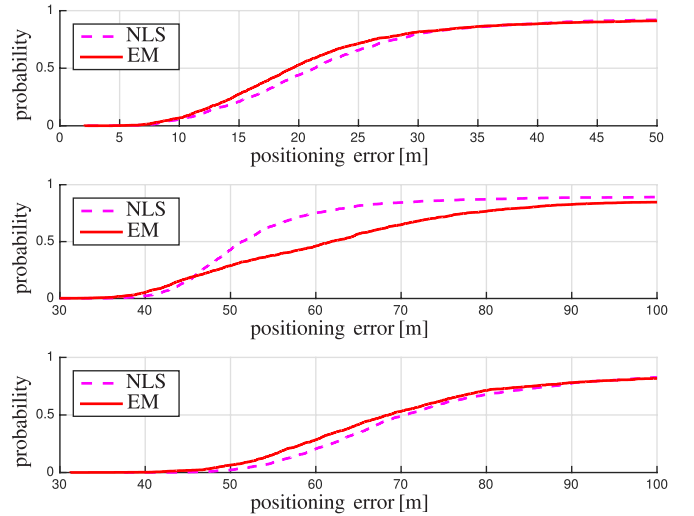


Fig. 4. Empirical CDFs of positioning errors for positioning tests of example topology. Upper plot shows the CDFs for the EPA5 channel model, plot in the middle shows CDFs for ETU70 channel model with TDE range $[-0.5 T_s, 0.5 T_s]$, and lower plot shows the CDFs for the ETU70 channel model with TDE range $[-0.5 T_s, 6 T_s]$.

two consecutive iterations in either of the algorithms are closer than 1 meter to each other, the corresponding algorithm is terminated and the current estimate $\hat{\mathbf{x}}$ is returned. To avoid infinite loops we use upper limits $n_{\text{EM}}^{\text{max}} = 50$, $n_{\text{dGN}}^{\text{max}} = 50$ and $n_{\text{NLS}}^{\text{max}} = 50$; and similar to Section IV-B, we use a maximum of 5 iterations to find a suitable scaling factor α .

For both methods, we assume a multivariate-normal prior distribution for \mathbf{x} with the mean being the center of the three most powerful BSs from which ranging measurements are available, i.e., the initial position estimate is considered at the barycenter of the three most powerful BSs, and the covariance matrix is $\mathbf{P} = 1000^2 \text{ m}^2 \mathbf{I}_{2 \times 2}$.

1) *Positioning Errors*: Fig. 4 shows the empirical CDFs of the positioning errors in the tests. The results are as expected for the EPA5 channel and for the ETU70 channel with TDE range $[-0.5 T_s, 6 T_s]$. For ETU70 with TDE range $[-0.5 T_s, 0.5 T_s]$ the results, however, differ from the results in Section IV-C.

An analysis of the errors in the ranging measurements used for positioning can partly explain these results. Fig. 5 shows the histograms of ranging errors in the measurements used for positioning (labeled as test data). The shape of the error distribution in training and test data is similar for the EPA5 channel, but the test data's histogram is shifted to the left. Both normal and skew-t distribution (fitted to the training data in Section IV-B) model the errors in the test data less precisely; their KLD values increase significantly. This means that there is a significant mismatch between the error models used by EM and NLS and the error distribution in the test data. Furthermore, the EM loses its edge over the NLS because both their error models are almost equally good (similar KLD values), which explains why the EM is not performing significantly better than the NLS for TDE range $[-0.5 T_s, 6 T_s]$.

For the ETU70 channel with TDE range $[-0.5 T_s, 0.5 T_s]$ normal and skew-t distribution have a similar KLD with

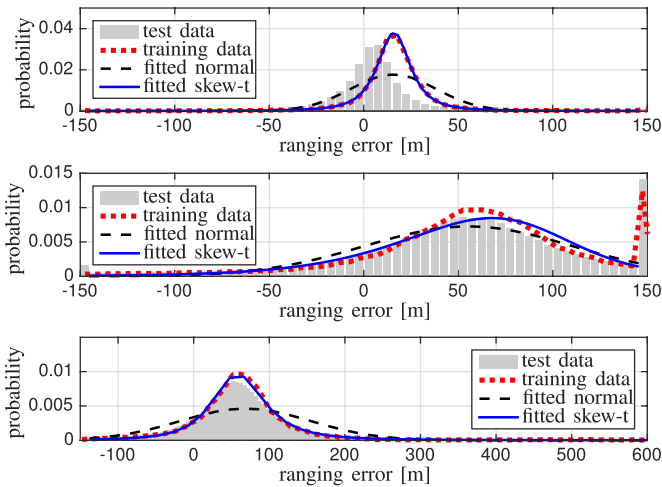


Fig. 5. Histogram of ranging errors in emulated LTE measurements for EPA5 (upper), and ETU70 channel with TDE range ranges $[-0.5 T_S, 0.5 T_S]$ (middle) and $[-0.5 T_S, 6 T_S]$ (lower; ranging errors above 600 meters are not displayed). Each figure contains in addition the empirical PDF of the training data and the PDFs of the normal and skew-t distribution fitted to the training data.

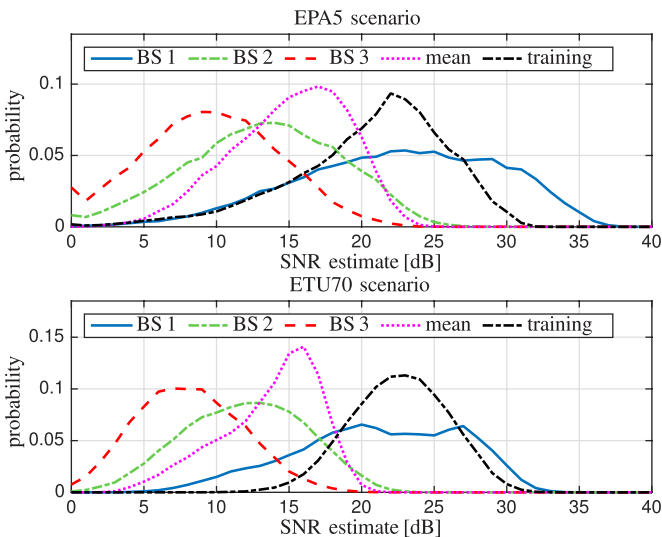


Fig. 6. SNR for test data of EPA5 (up) and ETU70 scenarios (down). Empirical PDFs of SNR values for strongest (*BS 1*), second-strongest (*BS 2*) and weakest BS (*BS 3*), average of all 3 BSs (*mean*) and in training data.

respect to the test data, which explains why the EM is not outperforming the NLS. However, it does not explain why the NLS performs better than the EM algorithm. This performance is mainly due to the impact of noise, which is discussed in the following section.

2) *Effect of SNR*: Another reason for the EM algorithm's poor performance seems to be the varying SNR in the positioning test. In the training the nominal SNR is around 24 dB. However, in the test data, the received power from each of the three BSs is different depending on the receiver location. Fig. 6 shows the PDFs of SNR estimates in the training data. In most of the cases the signal of BS 1 is the most powerful and the signal of BS 3 is the weakest. Thus, the noise affecting each ranging measurement may be more severe than the effect of

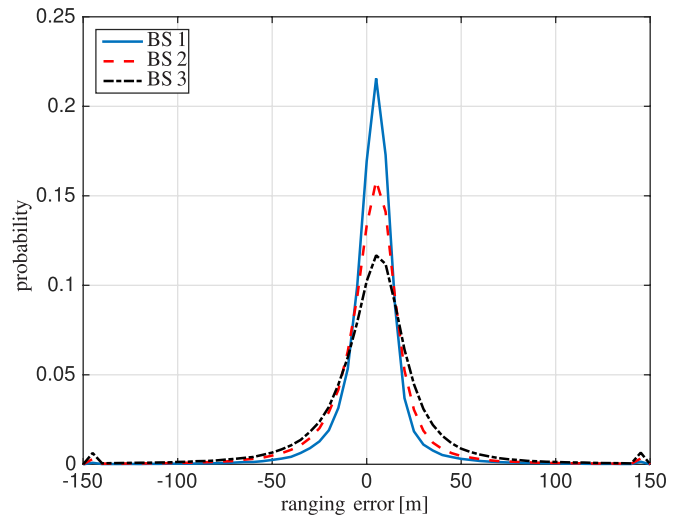


Fig. 7. Ranging error distribution for the three BSs in the EPA5 test.

multipath. As a result, the expected error distribution changes with respect to the prior distribution for the ranging measurement of each BS, decreasing the positioning performance of the statistical trilateration technique.

Fig. 6 shows also the histogram of the average SNR per three BSs and per radio frame, i.e., every 10 ms or every 14 measurements, for the EPA5 and ETU70 scenarios. These histograms are compared with the SNR histogram of the training data used in Section IV-B. As it can be seen, the SNR of BS 2 and 3 are lower than those used in the training scenario, which we used for fitting the parameters of normal and skew-t distribution. In addition, the SNR values for the EPA5 channel model are slightly higher than for the ETU70 channel model, because of the ETU70 model's more frequent fading events.

The ranging error distribution for the EPA5 channel model differs significantly for the three BSs (see Fig. 7). This means that the error distribution changes for varying SNR. For BS 1, which has high SNR values, it closely resamples a t-distribution, which is in line with our findings in Section IV-B (see Table II and Fig. 3). However, for low SNR values, which are observed for BS 3, the ranging error distribution closely resembles the normal distribution shown in Fig. 3.

An analysis of the performance of EM and NLS based on average SNR of the three BSs used for positioning reveals that for high average SNR the EM outperforms the NLS, but for low SNR the NLS yields similar or slightly better positioning accuracy. This analysis supports our belief that for low SNR the EM algorithm is unable to correctly infer the channel parameters given the high SNR training data. One way to address this problem would be to use a SNR-dependent error model. For example, we could fit the parameters of skew-t distributions to ranging error data with high SNR and to data with low SNR. In the positioning phase we would then choose one of the two error models or a combination based on the observed SNR.

The previous discussion also applies for the ranging error distribution obtained with the ETU70 tests, as is shown

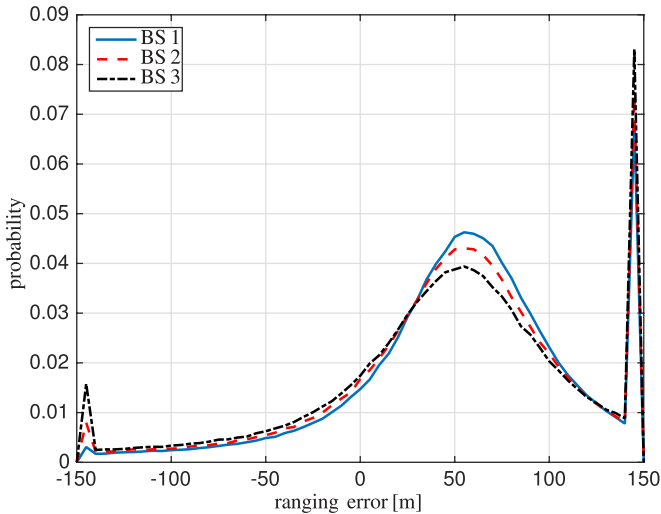


Fig. 8. Ranging error distribution for the three BSs in the ETU70 test with TDE range range $[-0.5 T_s, 0.5 T_s]$.

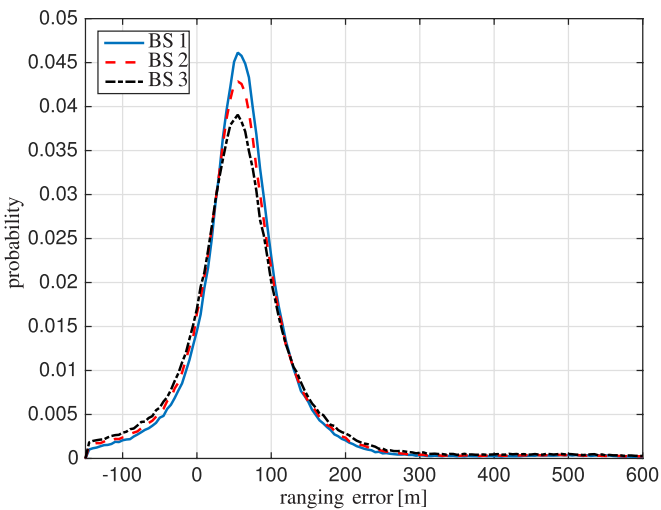


Fig. 9. Ranging error distribution for the three BSs in the ETU70 test with TDE range range $[-0.5 T_s, 6 T_s]$. Ranging errors above 600 meters are not displayed.

in Fig. 8 and Fig. 9. The variation of the SNR in the test data with respect to the calibration data introduces a mismodeling of the channel impact. As the noise increases, the ranging error distribution becomes wider, and a small bias is introduced towards the negative side of the distribution. The effect of this mismatch results in a significant degradation on the EM performance, which is higher for the large TDE range, i.e., $[-0.5 T_s, 6 T_s]$, than for reduced TDE range, i.e., $[-0.5 T_s, 0.5 T_s]$. The NLS algorithm only benefits from the increase of the impact of noise, inducing a Gaussian distribution, for the TDE range $[-0.5 T_s, 0.5 T_s]$. In contrast, the large deviations with the TDE range $[-0.5 T_s, 6 T_s]$ result in a worse performance of the NLS method with respect to the EM method. In a practical scenario, a restrictive TDE range, e.g. $[-0.5 T_s, 0.5 T_s]$, requires a very accurate acquisition or a robust tracking architecture, thus a large TDE range, e.g. $[-0.5 T_s, 6 T_s]$, is more common in order to cover most of the multipath delay spread. For instance, the TDE search window is set to twice the cyclic prefix length in [15], i.e.,

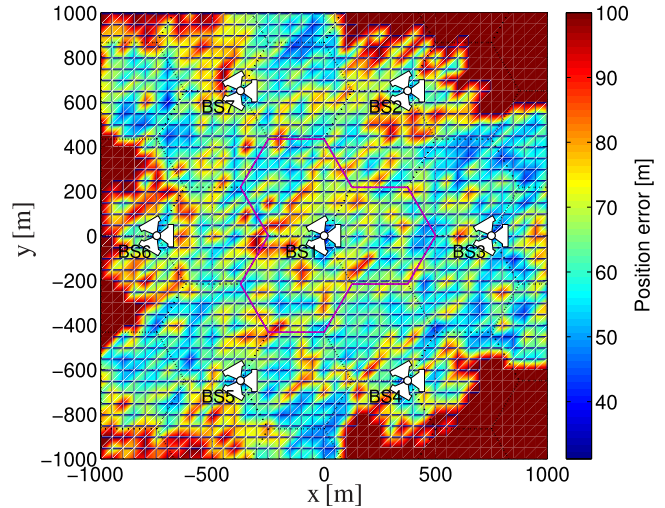


Fig. 10. Mean position error under ETU70 channel using EM algorithm, for which parameters were fitted to unrestricted data. Errors are limited to 150 meters. 65-degree sectors for each of the three antennas in each BS are denoted by triangles.

approximately $9 \mu s$. Thus, the proposed EM algorithm should be more applicable to practical conditions than the NLS algorithm, because it is shown to be more robust than the NLS for large deviations in the ranging errors, even if there is a mismatch in the ranging error model.

In Fig. 4 we notice that EM and NLS produce large position errors, i.e., above 100 meters, for 10% (EPA5) to 20% (ETU70) of the receiver locations. The analysis for the SNR effect reveals that those large positioning errors occur in locations with low average SNR from the three observed BSs. In order to get a better understanding under which circumstances both algorithms fail to provide reasonable position estimates, let us consider Fig. 10. It shows the EM position errors for all 1681 grid points in the ETU70 scenario, which used parameter estimates fitted to the whole training data. We limit the displayed errors to a maximum of 100 meters. Similar heat maps are obtained for the NLS and for the rest of scenarios, but they are not shown here due to space limitations. From the map we notice that the locations with poor position estimates are far from the prior position estimate, which was chosen to be the center of the 3 BSs observed in that location. The measurements do not provide significant additional information at these locations due to their low SNR [3]. Therefore, the posterior position estimate (i.e. the MAP estimate) will not differ significantly from the prior estimate, which results in a large positioning error.

3) *Consistency of Position Estimates*: Achieving high positioning accuracy in the dark red regions of Fig. 10 seems to be impossible or at least computationally unfeasible. However, one can try to detect those unreliable position estimates.

As an example, the unreliable position estimate can be detected if the SNR estimation is below a certain threshold. However, a better alternative can be based on the position estimate's covariance matrix, because it provides information on how certain the algorithm is about the position estimate. Since the EM yields the MAP estimate, this information is not directly available. The Gibbs sampler, which has been used

TABLE IV
AVERAGE NUMBER OF ITERATIONS USED BY dGN, EM AND
dGN USED INSIDE THE EM ALGORITHM (dGN-EM) IN
THE TEST WITH REALISTIC EMULATED LTE DATA

Channel	TDE	Method	5%-ile	Mean	95%-ile
EPA5	[-0.5, 0.5]	NLS	2.99	4.67	8.54
		EM	3.87	5.76	9.49
		dGN	2.00	2.31	3.02
ETU70	[-0.5, 0.5]	NLS	3.14	5.18	8.56
		EM	6.14	7.45	10.83
		dGN	2.25	2.76	3.81
ETU70	[-0.5, 6]	NLS	3.36	5.34	8.51
		EM	5.33	6.53	11.66
		dGN	2.37	2.84	3.68

for fitting the parameters of the skew-t distributions to the training data, could be used instead. It would yield a normal distribution for the position estimate. However, the GS is extremely slow. Thus, the most viable approach is to compute a covariance matrix inside the EM. An applicable approach is described in [43, pp. 114 ff.], where the authors show how to compute an approximation for the observed information matrix if measurement errors are assumed to be independently identically distributed.

4) *Complexity*: As mentioned above, the EM requires more computations than the NLS. Thus, let us look at the number of iterations used in both dGN and EM algorithms. In [22], the dGN and the EM have been analyzed with respect to the number of mathematical operations from 5 different classes they require. The overall numbers of mathematical operations required by dGN and EM are $\mathcal{O}(n_{\text{dGN}}K^3)$ and $\mathcal{O}(n_{\text{EM}}n_{\text{dGN}}K^3)$ respectively. Table IV shows the mean as well as the 5 and 95 percentile values of the average number (over the 70 positioning attempts) of iterations used in a single grid point. For our threshold values of 1 meter for NLS, dGN and EM, the EM and the NLS use more than the 4 iterations that we used in [22], while for the dGN that is applied inside the EM, in general, fewer than 3 iterations are necessary. Thus, in our tests the increase in computational demand when switching from the NLS to the EM is on a similar level as shown in [22], i.e., approximately five times higher.

5) *Influence of Measurement Quantity*: Finally, we want to summarize our results on the influence of number of measurements used for positioning. The accuracy of both NLS and EM improves if more than 4 measurements from each of the 3 BSs are used, and worsens if fewer than 4 measurements are used. The shapes of the positioning error CDFs are similar to the ones in Fig. 4. For the ETU70 scenarios the percentage of cases in which the EM performs better than the NLS increases slightly when fewer measurements are available. This can be explained by the fact that outliers are not so influential in NLS when there are many measurements, thus there is not so much advantage using a robust estimator like EM in its place.

V. CONCLUSIONS

In this paper we provide an extensive trial of the Expectation Maximization (EM) algorithm that was proposed in [22] for solving the trilateration problem in scenarios with

TOA-based range measurements and skew-t distributed measurement errors. The paper focuses on the evaluation of the EM algorithm's positioning performance using LTE ranging data obtained in a laboratory testbed with realistic conditions.

We start by fitting parameters of skew-t and normal distributions to ranging error data from two 3GPP standard channel models. The fitted skew-t distributions provide significantly better approximations for the error data than the fitted normal distributions (lower KLD and JSD values). When the errors in the range measurements follow the fitted skew-t distributions the EM algorithm outperforms a standard Nonlinear Least Squares (NLS) algorithm. In the error quantiles we see improvements of up to 43%.

However, if the channel conditions during generation of calibration data and test data differ, then the EM does not necessarily provide better positioning accuracy than the NLS algorithm. Changes in the channel conditions cause changes in the ranging error distribution. Therefore, the error model used in the EM algorithm, the skew-t distribution, is not correct anymore, which results in a weaker positioning accuracy of the EM algorithm. This also happens for the NLS algorithm's error model, the normal distribution, which is not correct due to the model mismatch. However, because the skew-t distribution provides a better fit than the normal distribution to the calibration data due to the use of two additional parameters, it is more vulnerable to changing patterns in the error distributions.

We notice a significant mismatch in the error distributions of calibration and test data for the EPA5 channel model, which explains the EM algorithm's poorer performance than the expected positioning accuracy. Our analysis shows that for the EPA5 channel model the ranging error distribution depends strongly on the measurements' SNR. Thus, to improve the EM accuracy one could modify the algorithm such that it uses a SNR-dependent skew-t error model. Developing such an algorithm is left for further research.

The analysis of the ETU70 channel model shows a high impact of the multipath delay spread on the ranging error distribution. For this channel model, the EM suffers when only one sampling period of time-delay estimation range is used, because then large positive ranging errors are not captured. These ranging errors stem mostly from NLoS range measurements, which are usually larger than the true distance between transmitter and receiver [5]. The probability of NLoS in the ETU70 model is around 37% (for the EPA5 model it is only 13%). By increasing the estimation range (in order to cover most of the delay spread), the EM regains its edge over the NLS.

To summarize, the proposed EM algorithm is shown to be more robust than the NLS for large deviations in the ranging errors. The EM algorithm uses the NLS in its M-step; and for the E-step closed-form equations are presented in this paper. However, future work should compare the EM algorithm and the skew-t error model with other algorithms and distributions proposed in the literature in terms of positioning accuracy and computational demand. Furthermore, its applicability to received signal strength and direction of arrival-based trilateration could also be investigated.

REFERENCES

- [1] *E-UTRAN; Stage 2 Functional Specification UE Positioning E-UTRAN, Std., Rel. 13*, document 3GPP TS 36.305, 2015.
- [2] *E-UTRA; Physical Channels Modulation, Std., Rel. 9*, document 3GPP TS 36.211, 2009.
- [3] M. Z. Win *et al.*, “Network localization and navigation via cooperation,” *IEEE Commun. Mag.*, vol. 49, no. 5, pp. 56–62, May 2011.
- [4] D. Dardari, C.-C. Chong, and M. Z. Win, “Threshold-based time-of-arrival estimators in UWB dense multipath channels,” *IEEE Trans. Commun.*, vol. 56, no. 8, pp. 1366–1378, Aug. 2008.
- [5] D. Dardari, A. Conti, U. Ferner, A. Giorgetti, and M. Z. Win, “Ranging with ultrawide bandwidth signals in multipath environments,” *Proc. IEEE*, vol. 97, no. 2, pp. 404–426, Feb. 2009.
- [6] I. Güvenc and C.-C. Chong, “A survey on TOA based wireless localization and NLOS mitigation techniques,” *IEEE Commun. Surveys Tuts.*, vol. 11, no. 3, pp. 107–124, 3rd Quart., 2009.
- [7] S. Marano, W. M. Gifford, H. Wymeersch, and M. Z. Win, “NLOS identification and mitigation for localization based on UWB experimental data,” *IEEE J. Sel. Areas Commun.*, vol. 28, no. 7, pp. 1026–1035, Sep. 2010.
- [8] H. Chen, G. Wang, Z. Wang, H. C. So, and H. V. Poor, “Non-line-of-sight node localization based on semi-definite programming in wireless sensor networks,” *IEEE Trans. Wireless Commun.*, vol. 11, no. 1, pp. 108–116, Jan. 2012.
- [9] Z. Xiao, H. Wen, A. Markham, N. Trigoni, P. Blunsom, and J. Frolik, “Non-line-of-sight identification and mitigation using received signal strength,” *IEEE Trans. Wireless Commun.*, vol. 14, no. 3, pp. 1689–1702, Mar. 2015.
- [10] H. Tang, Y. Park, and T. Qiu, “A TOA-AOA-based NLOS error mitigation method for location estimation,” *EURASIP J. Adv. Signal Process.*, vol. 2008, no. 1, 2007, Art. no. 682528.
- [11] C. K. Seow and S. Y. Tan, “Non-line-of-sight localization in multipath environments,” *IEEE Trans. Mobile Comput.*, vol. 7, no. 5, pp. 647–660, May 2008.
- [12] S. Al-Jazzar, M. Ghogho, and D. McLernon, “A joint TOA/AOA constrained minimization method for locating wireless devices in non-line-of-sight environment,” *IEEE Trans. Veh. Technol.*, vol. 58, no. 1, pp. 468–472, Jan. 2009.
- [13] M. Z. Win and Y. Shen, “On the accuracy of localization systems using wideband antenna arrays,” *IEEE Trans. Commun.*, vol. 58, no. 1, pp. 270–280, Jan. 2010.
- [14] Y. Xie, Y. Wang, B. Wu, and X. You, “Mobile localisation with TOA, AOA and doppler estimation in NLOS environments,” *Trans. Emerg. Telecommun. Technol.*, vol. 23, no. 6, pp. 499–507, 2012.
- [15] W. Xu, M. Huang, C. Zhu, and A. Dammann, “Maximum likelihood TOA and OTDOA estimation with first arriving path detection for 3GPP LTE system,” *Trans. Emerg. Telecommun. Technol.*, vol. 27, no. 3, pp. 339–356, 2016.
- [16] J. A. del Peral-Rosado, J. A. López-Salcedo, G. Seco-Granados, F. Zanier, and M. Crisci, “Joint maximum likelihood time-delay estimation for LTE positioning in multipath channels,” *EURASIP J. Adv. Signal Process.*, vol. 2014, no. 33, p. 13, Feb. 2014.
- [17] X. Li and K. Pahlavan, “Super-resolution TOA estimation with diversity for indoor geolocation,” *IEEE Trans. Wireless Commun.*, vol. 3, no. 1, pp. 224–234, Jan. 2004.
- [18] P. Müller, H. Wymeersch, and R. Piché, “UWB positioning with generalized Gaussian mixture filters,” *IEEE Trans. Mobile Comput.*, vol. 13, no. 10, pp. 2406–2414, Oct. 2014.
- [19] M. Kok, J. D. Hola, and T. B. Schön, “Indoor positioning using ultrawideband and inertial measurements,” *IEEE Trans. Veh. Technol.*, vol. 64, no. 4, pp. 1293–1303, Apr. 2015.
- [20] N. A. Alsindi, B. Alavi, and K. Pahlavan, “Measurement and modeling of ultrawideband TOA-based ranging in indoor multipath environments,” *IEEE Trans. Veh. Technol.*, vol. 58, no. 3, pp. 1046–1058, Mar. 2009.
- [21] B. Alavi and K. Pahlavan, “Modeling of the distance error for indoor geolocation,” in *Proc. IEEE Wireless Commun. Netw. Conf. (WCNC)*, vol. 1, Mar. 2003, pp. 668–672.
- [22] P. Müller and R. Piché, “Statistical trilateration with skew-t errors,” in *Proc. Int. Conf. Localization GNSS (ICL-GNSS)*, Jun. 2015, pp. 1–6.
- [23] R. Piché, “Estimation of model parameters,” in *Mathematical Modeling With Multidisciplinary Applications*, X.-S. Yang, Ed. New York, NY, USA: Wiley, 2013, pp. 169–190.
- [24] A. Azzalini, *The Skew-Normal and Related Families*. Cambridge, U.K.: Cambridge Univ. Press, 2014.
- [25] T. I. Lin, J. C. Lee, and W. J. Hsieh, “Robust mixture modeling using the skew t distribution,” *Statist. Comput.*, vol. 17, no. 2, pp. 81–92, Jun. 2007.
- [26] A. E. Gelfand and A. F. Smith, “Sampling-based approaches to calculating marginal densities,” *J. Amer. Statist. Assoc.*, vol. 85, no. 410, pp. 398–409, 1990.
- [27] *E-UTRA; User Equipment (UE) Radio Transmission Reception, Std., Rel. 9*, document 3GPP TS 36.101, 2014.
- [28] *E-UTRA; Study 3D Channel Model for LTE, Std., Rel. 12*, document 3GPP TR 36.873, 2015.
- [29] J. A. del Peral-Rosado, J. A. López-Salcedo, G. Seco-Granados, F. Zanier, and M. Crisci, “Analysis of positioning capabilities of 3GPP LTE,” in *Proc. 25th Int. Tech. Meeting Satellite Division ION*, Sep. 2012, pp. 650–659.
- [30] L. Xu and M. I. Jordan, “On convergence properties of the EM algorithm for Gaussian mixtures,” *Neural Comput.*, vol. 8, no. 1, pp. 129–151, 1996.
- [31] A. P. Dempster, N. M. Laird, and D. B. Rubin, “Maximum likelihood from incomplete data via the EM algorithm,” *J. Roy. Statist. Soc. B (Methodol.)*, vol. 39, no. 1, pp. 1–38, 1977.
- [32] J. Sanz, J. M. Juan, and M. Hernández-Pajares, *GNSS Data Processing: Fundamentals and Algorithms*, vol. 1. Noordwijk, The Netherlands: ESA Communications, 2013. [Online]. Available: http://www.navipedia.net/GNSS_Book/ESA_GNSS-Book_TM-23_Vol_1.pdf
- [33] C. Mehlhührer, J. C. Ikuno, M. Šimko, S. Schwarz, M. Wrulich, and M. Rupp, “The Vienna LTE simulators—Enabling reproducibility in wireless communications research,” *EURASIP J. Adv. Signal Process.*, vol. 2011, no. 29, pp. 1–14, 2011.
- [34] J. A. del Peral-Rosado, J. A. López-Salcedo, F. Zanier, and M. Crisci, “Achievable localization accuracy of the positioning reference signal of 3GPP LTE,” in *Proc. Int. Conf. Localization GNSS (ICL-GNSS)*, Jun. 2012, pp. 1–6.
- [35] *E-UTRA; Radio Frequency (RF) System Scenarios, Std., Rel. 9*, document 3GPP TR 36.942, 2012.
- [36] J. A. del Peral-Rosado *et al.*, “Comparative results analysis on positioning with real LTE signals and low-cost hardware platforms,” in *Proc. 7th ESA Workshop Satellite Navigat. Technol. (NAVITEC)*, Dec. 2014, pp. 1–8.
- [37] J. A. del Peral-Rosado, J. López-Salcedo, G. Seco-Granados, P. Crosta, F. Zanier, and M. Crisci, “Downlink synchronization of LTE base stations for opportunistic ToA positioning,” in *Proc. Int. Conf. Localization GNSS (ICL-GNSS)*, Jun. 2015, pp. 1–6.
- [38] Y. Li, “Blind SNR estimation of OFDM signals,” in *Proc. IEEE Int. Conf. Microw. Millim. Wave Technol. (ICMMT)*, May 2010, pp. 1792–1796.
- [39] T. M. Cover and J. A. Thomas, *Elements of Information Theory*, 1st ed. New York, NY, USA: Wiley, 1991.
- [40] J. Lin, “Divergence measures based on the Shannon entropy,” *IEEE Trans. Inf. Theory*, vol. 37, no. 1, pp. 145–151, Jan. 1991.
- [41] S. Bartoletti, W. Dai, A. Conti, and M. Z. Win, “A mathematical model for wideband ranging,” *IEEE J. Sel. Topics Signal Process.*, vol. 9, no. 2, pp. 216–228, Mar. 2015.
- [42] (Sep. 2013). *JAGS—Just Another Gibbs Sampler*. [Online]. Available: <http://mcmc-jags.sourceforge.net>
- [43] G. J. McLachlan and T. Krishnan, *The EM Algorithm and Extensions*, 2nd ed. New York, NY, USA: Wiley, 2008.



Philipp Müller received the B.Sc. and M.Sc. degrees in mathematics from the Chemnitz University of Technology, Germany, in 2007 and 2010, respectively. He is currently pursuing the Ph.D. degree with the Department of Automation Science and Engineering, Tampere University of Technology, Finland. He has been a Visiting Researcher with the Universitat Autònoma de Barcelona, Spain, in autumn 2014. His research interests are mathematical modeling, Bayesian statistics, and algorithms for low-complexity positioning in terrestrial radio networks.



José A. del Peral-Rosado (S'12–M'15) received the Ph.D. degree in telecommunications engineering from the Universitat Autònoma de Barcelona (UAB) in 2014. Since 2014, he has been a Post-Doctoral Researcher with the Department of Telecommunications and Systems Engineering, UAB, and holds a grant from the European Space Agency (ESA) under the NPI programme. From 2014 to 2016, he was a Visiting Researcher with the European Space Research and Technology Centre, ESA. His research interests are in signal processing with applications to communications and navigation, hybrid satellite and terrestrial localization, and synchronization techniques and positioning with GNSS, 4G LTE, and 5G systems.



Gonzalo Seco-Granados (S'97–M'02–SM'08) received the Ph.D. degree in telecommunications engineering from the Universitat Politècnica de Catalunya in 2000, and the M.B.A. degree from IESE in 2002. From 2002 to 2005, he was a member of the Technical Staff of the European Space Agency, where he was involved in the design of the Galileo system. Since 2006, he has been an Associate Professor with the Department of Telecommunications and Systems Engineering, Universitat Autònoma de Barcelona. He has authored over 180 papers and has been a Principal Investigator of over 25 research projects. In 2015, he was a Fulbright Visiting Professor with the University of California at Irvine. His research interests are the design of signals and reception techniques for satellite-based and terrestrial localization systems, multiantenna receivers, and positioning with 5G technologies.



Robert Piché (M'10–SM'16) received the B.A.Sc., M.A.Sc., and Ph.D. degrees from the University of Waterloo, Canada, in 1981, 1982, and 1986, respectively, all in civil engineering. He was an Assistant Professor of Mathematics with the École Polytechnique de Montréal from 1986 to 1988. Since 1988, he has been with the Tampere University of Technology, Finland, where he has been a Professor since 2004. His scientific interests include mathematical modeling, numerical analysis, estimation theory, and positioning technology.